Supporting information

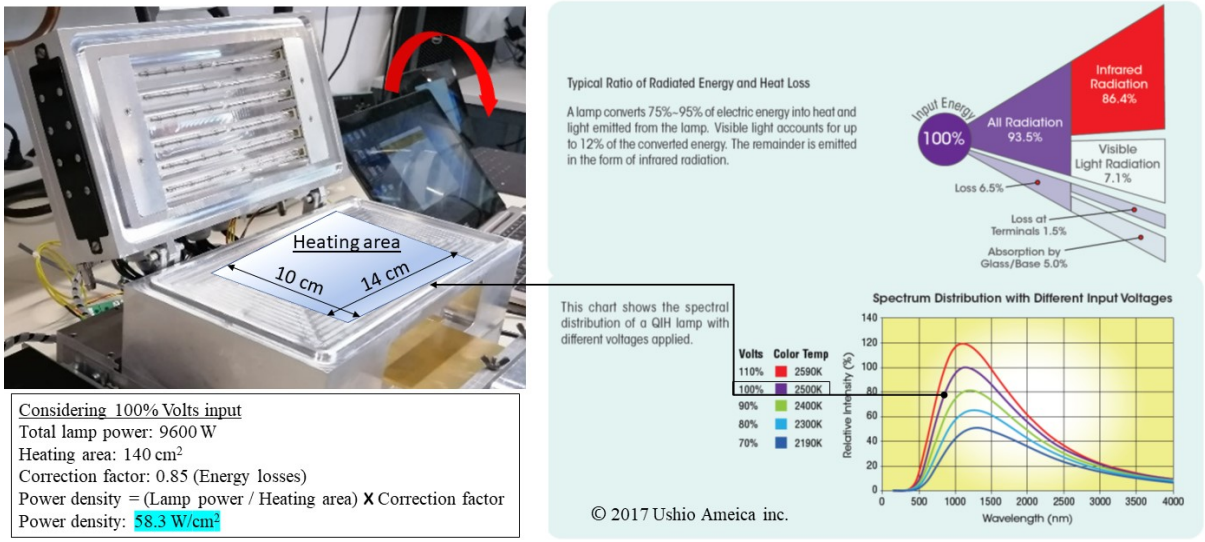

Considering 100% Volts input
Total lamp power: 9600 W
Heating area: 140 cm^2
Correction factor: 0.85 (Energy losses)
Power density = (Lamp power / Heating area) X Correction factor
Power density: 58.3 W/cm^2

Figure SI 1. Schematic of the power density estimation of the photonic source.

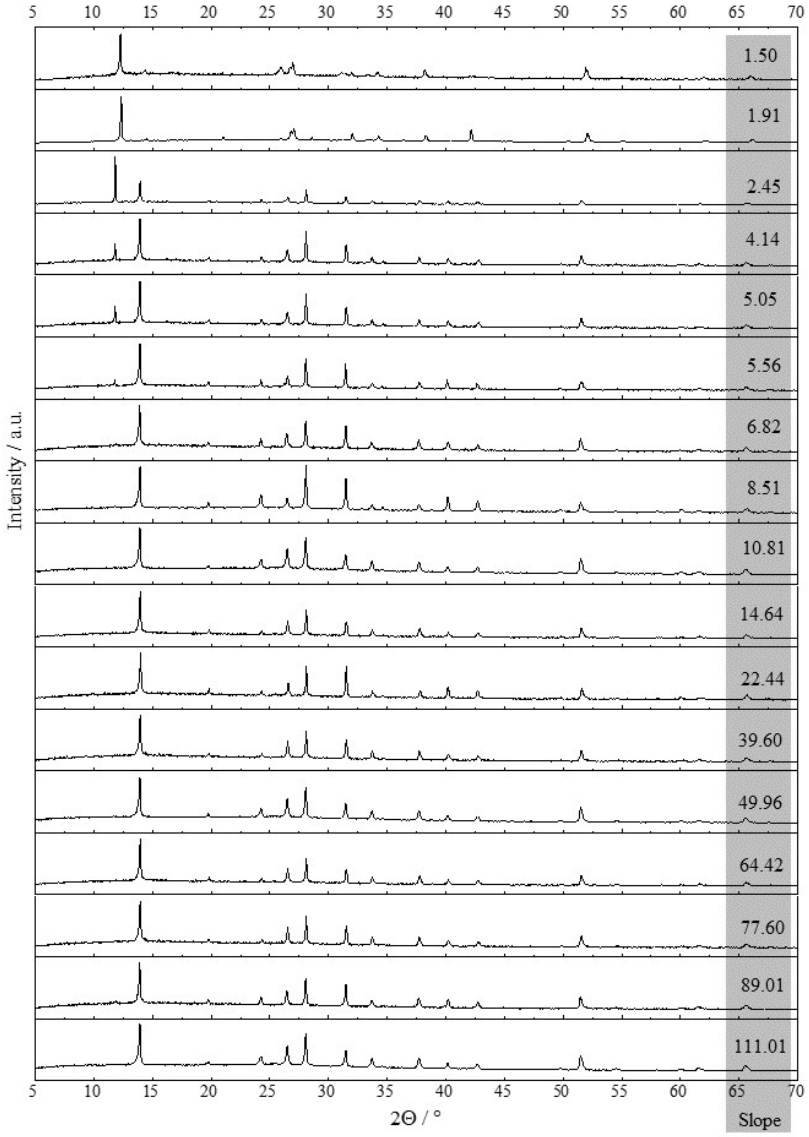

Figure SI 2. XRD diffraction patterns of 17 analyzed films.

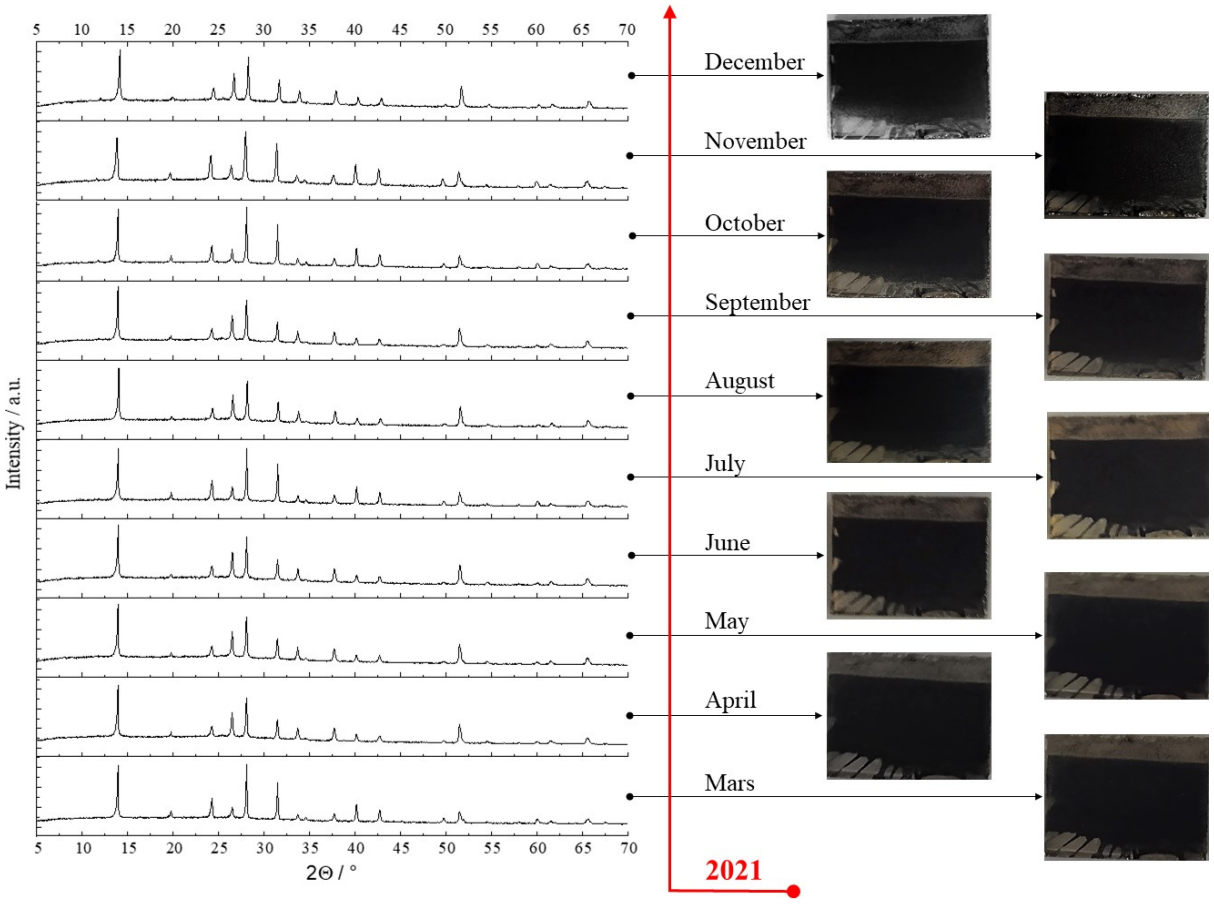

Figure SI 3. XRD diffraction patterns and indexed pictures of the 111.01 slope-heating rate film taken during ten months.

			Rwp
*I*4/*mcm*	8.9475(7)	12.7039(9)	7.3
*P*4/*m*	6.3321(4)	6.3478(4)	6.9
*P*4*bm*	6.3425(5)	6.3544(5)	7.0
*Pm*3-*m*	6.339(1)		9.2

Table SI 1. Unit cell calculated parameters of the $FAPbI_3$ black phase, fitted for different unit cell symmetries. Notably the fit is worse for the *Pm*-3*m*, as evidenced by the significantly higher *R*-value.

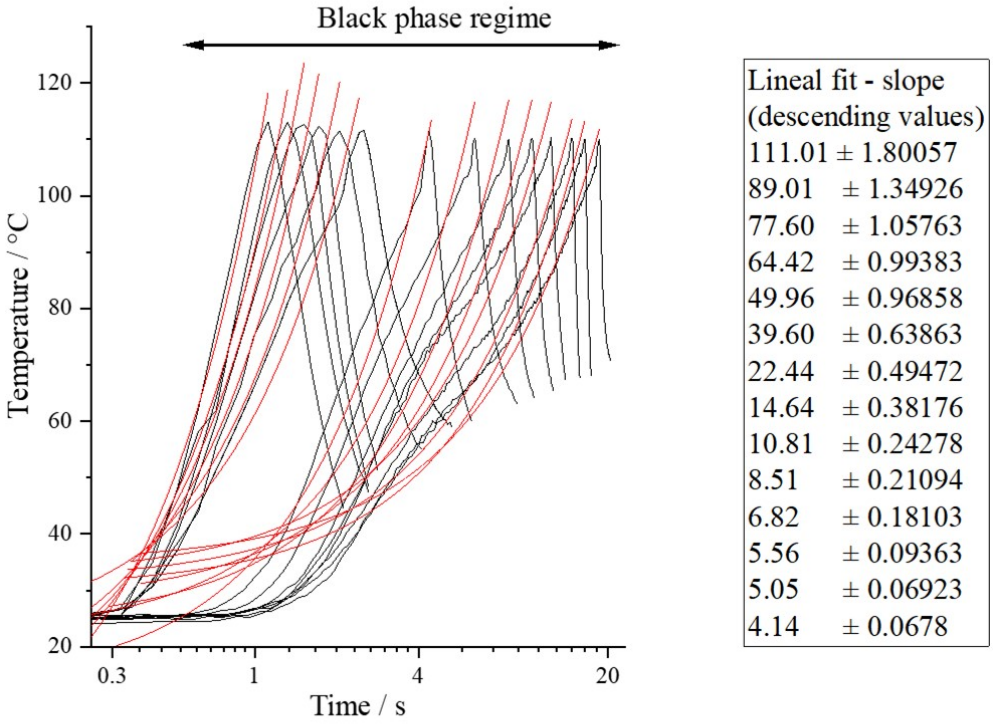

Figure SI 4. Temperature profile of the annealed sample in the black phase regime (logarithm scale).

samples slope ref. →	111.01	77.60	49.96
Data points	14’288’000	14’288’000	14’288’000
Ra /nm	97.07	148.94	216.52
Rp /nm		2193.91	2703.75
Rq /nm		218.77	289.55
Rt /nm		2631.57	3498.22
Rv /nm		-619.43	-794.46

Table SI 2. Statistical values of the profilometer measurements

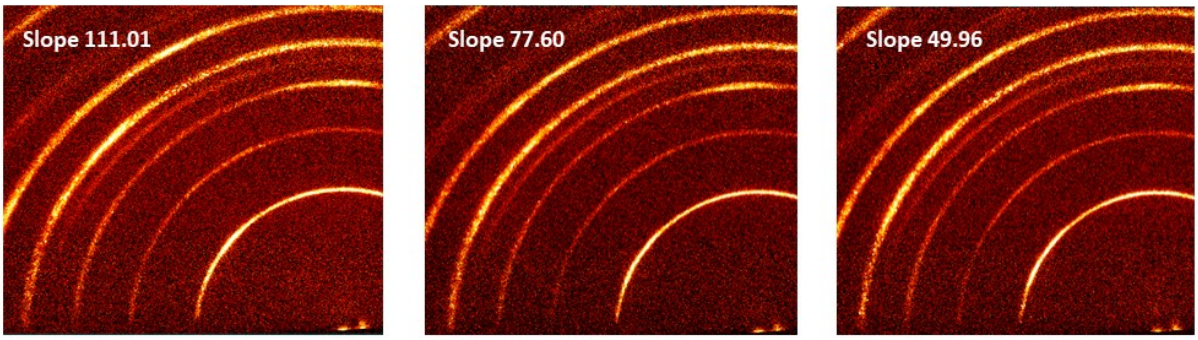

Figure SI 5. c) 2D GIWAXS images of the slope-rate processed selected films.

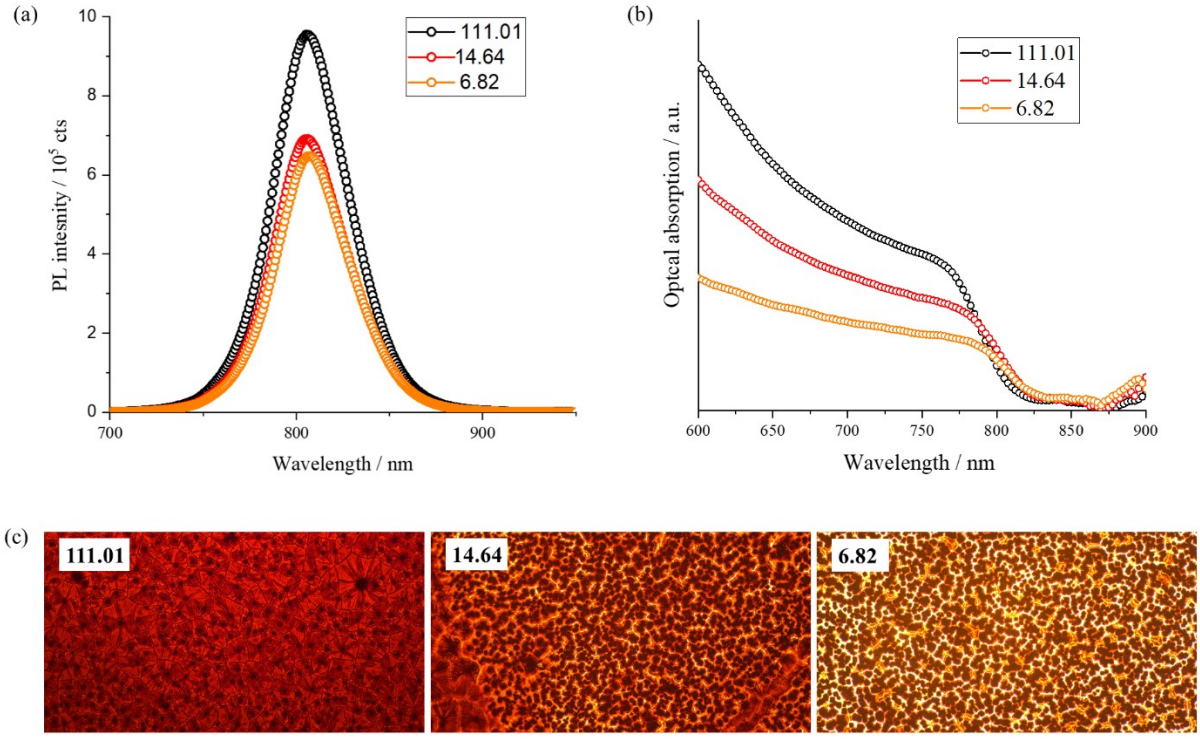

Figure SI 6. a) PL, b) absorption spectrum, and c) optical images of three heating rates – slopes processed films.

Model	Exponential
Equation	$y = y_0 + A*\exp(R_0*x)$
y_0	6.29125 ± 0.00418
A	6.56982E-7 ± 3.68559E-9
R_0	0.18857 ± 5.71361E-5
Reduced Chi-Sq	0.00942
R-Square (COD)	0.99998
Adj. R-Square	0.99998

Table SI 3. Parameters given by exponential curve fitting

Images (111.01 slope)	Number of grains	Area average/ μm^2	Radius average / μm
1	365	5360.03	41.31
2	213	9204.10	54.13
3	213	9167.73	54.02
4	298	6553.70	45.67
5	245	7999.64	50.46
6	269	7262.18	48.08
7	400	4894.35	39.47
8	323	6060.04	43.92
9	271	7227.35	47.96
10	194	10089.54	56.67
Total averages →	**333**	**8768.58**	**52.69**

Table SI 4. Collected parameters of the 140 optical images processed.

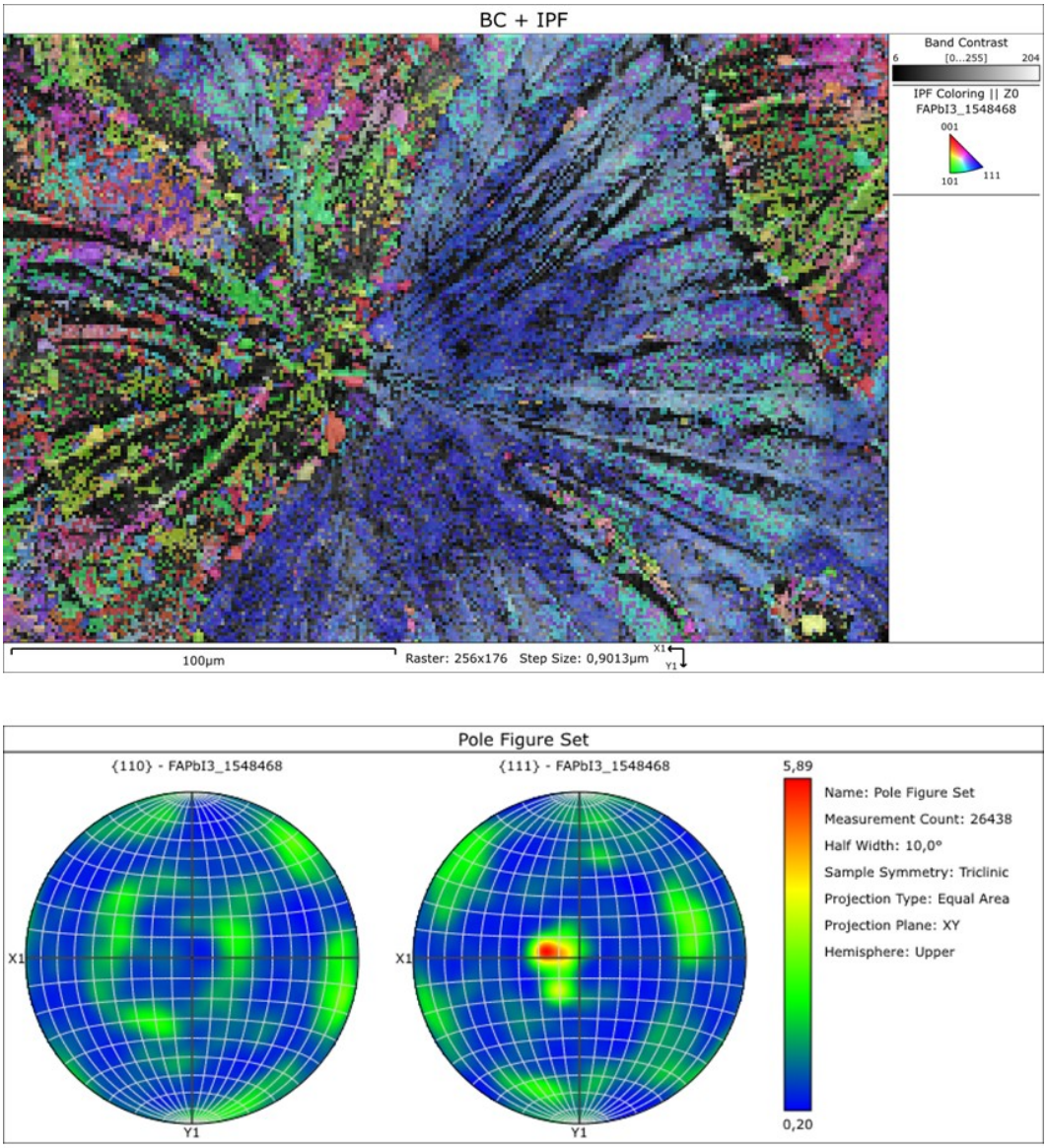

Figure SI 7. EBSD mapping of the 111.01 slope processed film (up) with their respective pole figure (down). The Multiple of Uniform Distribution (MUD) value in the pole figures is between 3 and 4, which corresponds to a weak-moderate texture.

TR-FLIM and decay time maps measurements

The TR-FLIM system was used to obtain images at a certain delay after the laser pulse, and with a certain integration time called gate-width. The list of temporal delays and gate widths used is the following:

Frames	Delay (ns)	Gate Width (ns)
1	0	3
2	180	10

3	280	30
4	480	60
5	780	100
6	1280	100
7	1780	100
8	2280	300
9	2780	300
10	3280	500
11	4280	500

The adjusted time is then computed as : delay + gatewidth/2. The corresponding laser reflection and PL images for the 11 frames are shown in Figure SI 9.

To obtain the decay time maps we fit a bi-exponential decay locally on the TR-FLIM cubes, the fitting interval was set to [800;3000] ns in terms of adjusted times - see Figure SI 11. The decay time map image is then obtained as the long characteristic time of the bi-exponential decay, see Figure SI 10.

To obtain the composite maps shown in the main text, we merge the laser reflection image to the long decay time image. We obtain the composite image by multiplying the color value of each pixel of the decay time map by the intensity of this pixel in the reflection image. This composite image gives qualitative information on both morphology and decay time.

Discussion of the impact of thickness - Case of similar surface recombination velocities.

In the case of negligible bottom surface recombination, the change of thickness could cause a change of observed decay time via for instance:[80]

$$\frac{1}{\tau} = \frac{1}{\tau_{bulk}} + \frac{S}{d}$$

where τ is the observed decay time, τ_{bulk} the SRH decay time due to bulk recombination, S the top surface recombination velocity, and d the local thickness. This simple formula shows that thinner location could lead to lower decay time if the surface recombination is constant. If we consider two regions: one with high thickness d_1 and high decay time τ_1 and another with smaller thickness d_2 and smaller decay time τ_2, we can show that the ratio between d_1 and d_2 is limited if we consider constant surface recombination S by:

$$1 - \frac{\tau_2}{\tau_1}\left(\frac{\tau_2}{\tau_1} - 1\right) \leq \frac{d_1}{d_2} \leq \frac{\tau_1}{\tau_2}$$

If we consider $\tau_1 = 500\text{ns}$ and $\tau_2 = 250\text{ns}$ as seen in Figure SI 10(c), then we can show that the difference in thickness between the high decay time regions and the low decay time regions is:

$$1.25 \leq \frac{d_1}{d_2} \leq 2 \quad \text{or} \quad 0.5 \leq \frac{d_2}{d_1} \leq 0.8$$

Discussion of the impact of thickness - Case of distinct surface recombination velocities.

One can compute the ratio of surface recombination in the case where they are not assumed equal. In this case we consider (see Figure 3 of the main paper for the decay times, and Figure 2 for the thicknesses):

- Region 1 : core of the domain;
  - $\tau_1 \approx 500\text{ns}$
  - $d_1 \approx 700\text{nm}$
- Region 2 : “valley”;
  - $\tau_2 \approx 250\text{ns}$
  - $d_2 \approx 350\text{nm}$

In this case, one can show that the ratio of surface recombination velocities of the core (S1) and of the valley (S2) are above:

$$\frac{S_2}{S_1} = \frac{d_2}{d_1} \times \frac{\frac{1}{\tau_2} - \frac{1}{\tau_{bulk}}}{\frac{1}{\tau_1} - \frac{1}{\tau_{bulk}}} \geq \frac{d_2}{d_1} \times \frac{\tau_1}{\tau_2} \approx 1 \qquad \text{(Eq S1)}$$

The far right value of this equation is the limit of the ratio in the case of negligible bulk recombination. Any additional bulk recombination would increase the ratio. For instance, if we assume a bulk lifetime of 1µs, then the ratio of surface recombination would equal 150%. It is therefore highly likely that the “valley” region has higher surface recombination than the “core” of the micro domain.

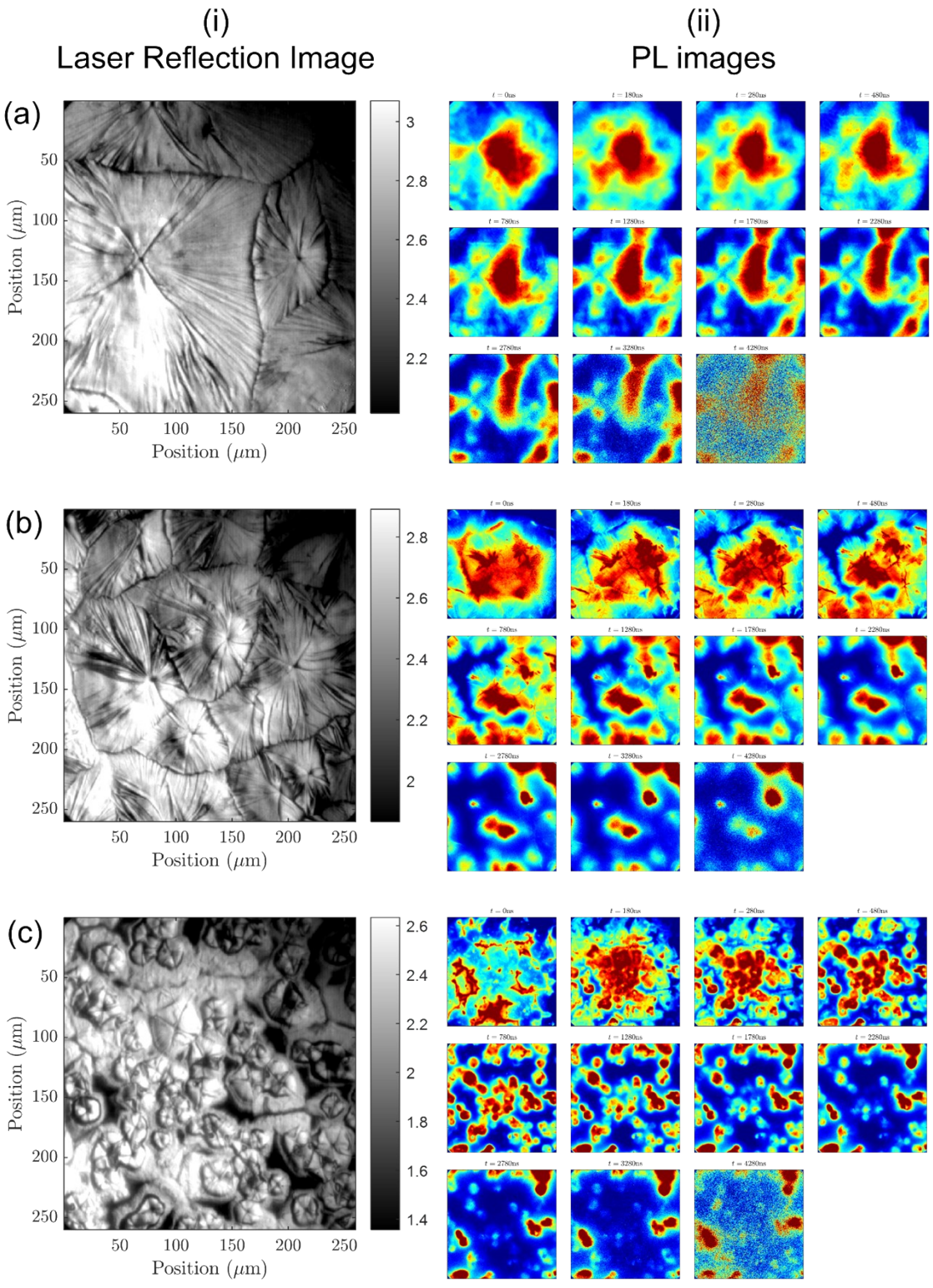

Figure SI 8: Raw data for the fast slope decay time map. (i) Laser reflection image. (ii) PL images at different times (and with different integration times, not shown) after the laser pulse. Each image is scaled with its own maximum. (a) Slope 111.01 (b) 77.60 (c) 49.96.

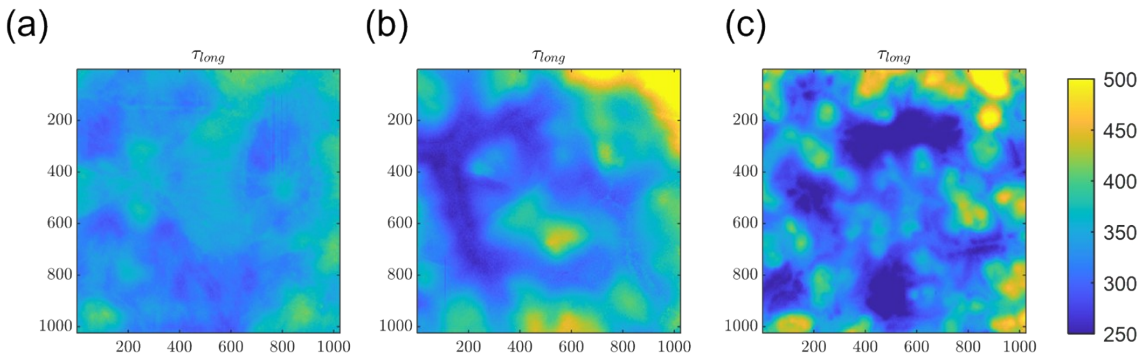

Figure SI 9: long decay time (in ns) maps obtained with the described procedure. (a) Slope 111.01 (b) 77.60 (c) 49.96.

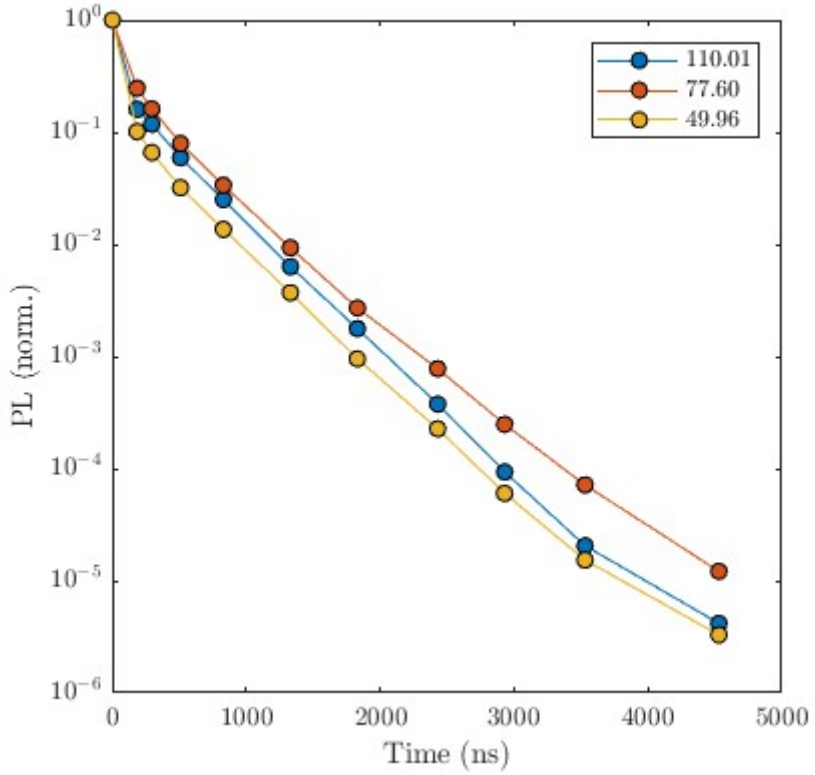

Figure SI 10: Decays of the average signal for the three data cubes. Each of the points corresponds to the images shown in Figure SI 9.

Hyperspectral and cw-PL spatial map measurements

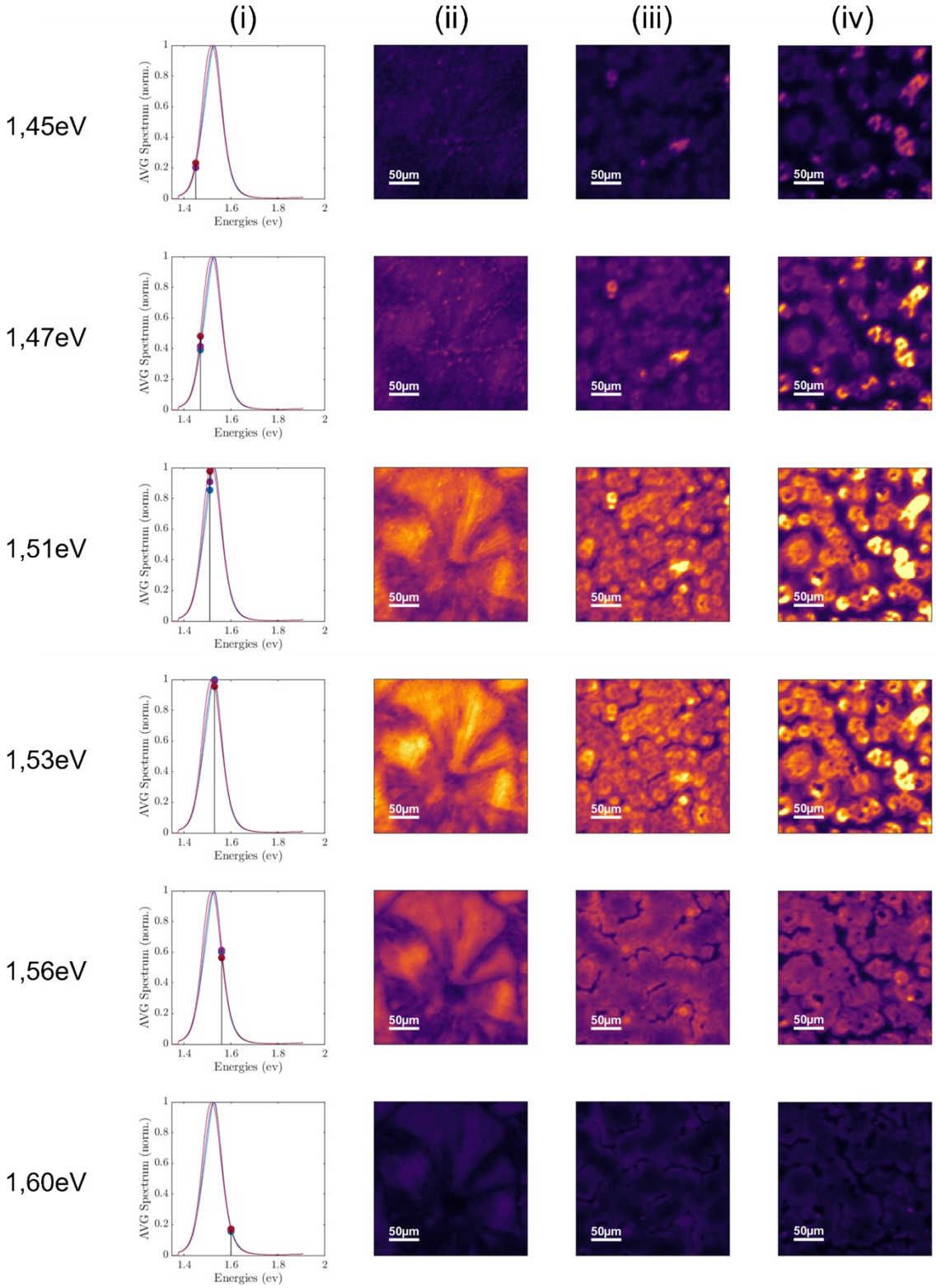

Figure SI 11: Hyperspectral **raw** data cube. Column (i) shows the three average spectra normalized as well as the selected wavelength. Column (ii), (iii), (iv) correspond to the images of PL emission at the selected energy (+- 0.01eV). (ii) Slope 111.01 (iii) 77.60 (iv) 49.96. Images are normalized by the maximal value of the average spectrum multiplied by 2.

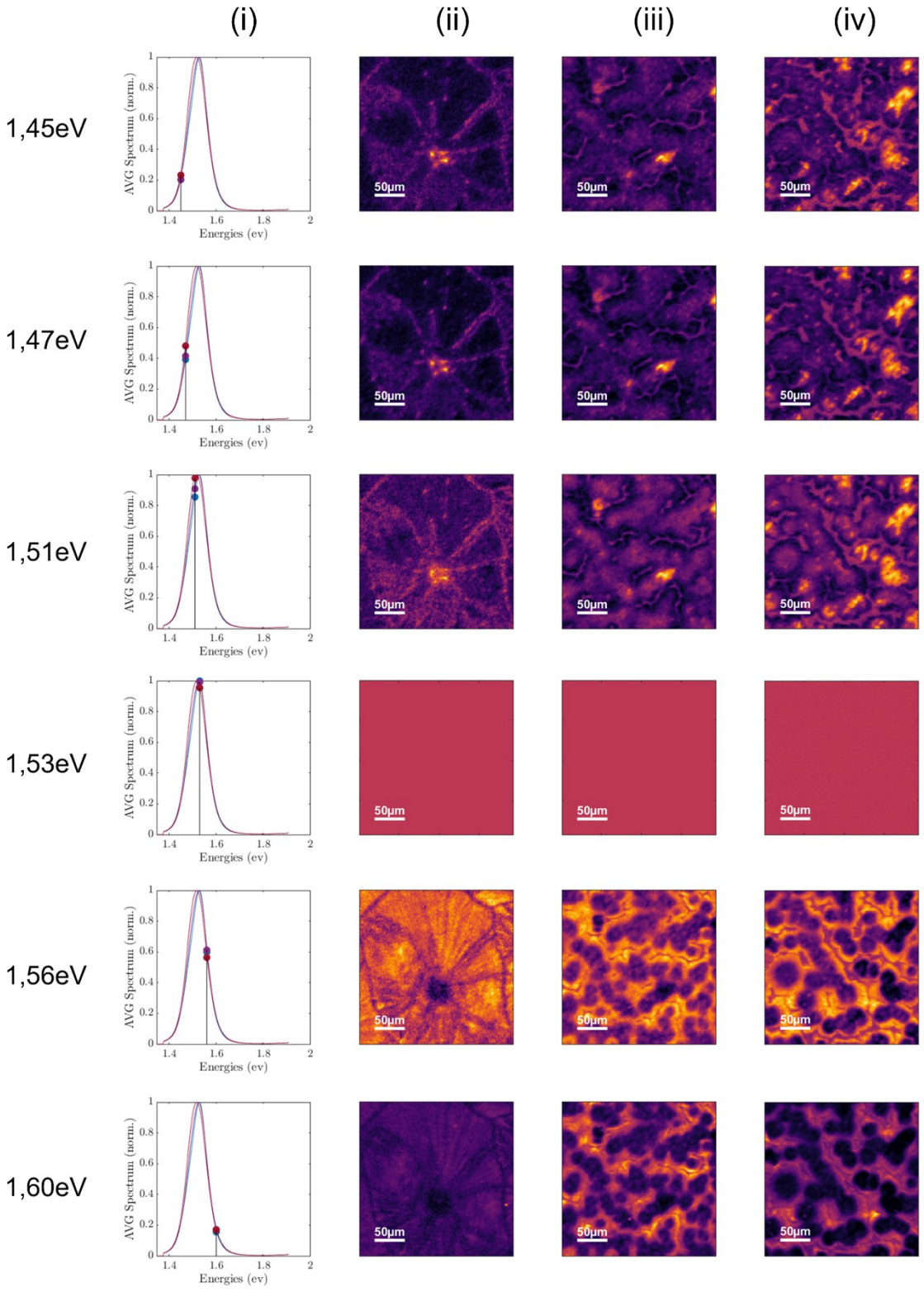

Figure SI 12: Hyperspectral **relative** data cube (all images are divided pixel by pixel by the image of emission at E=1.53eV). Column (i) shows the three average spectra normalized as well as the selected wavelength. Column (ii), (iii), (iv) correspond to the images of PL emission at the selected energy (+- 0.01eV). (ii) Slope 111.01 (iii) 77.60 (iv) 49.96. Images are normalized by the image at E=1.53eV. Color scales are not comparable with each other.

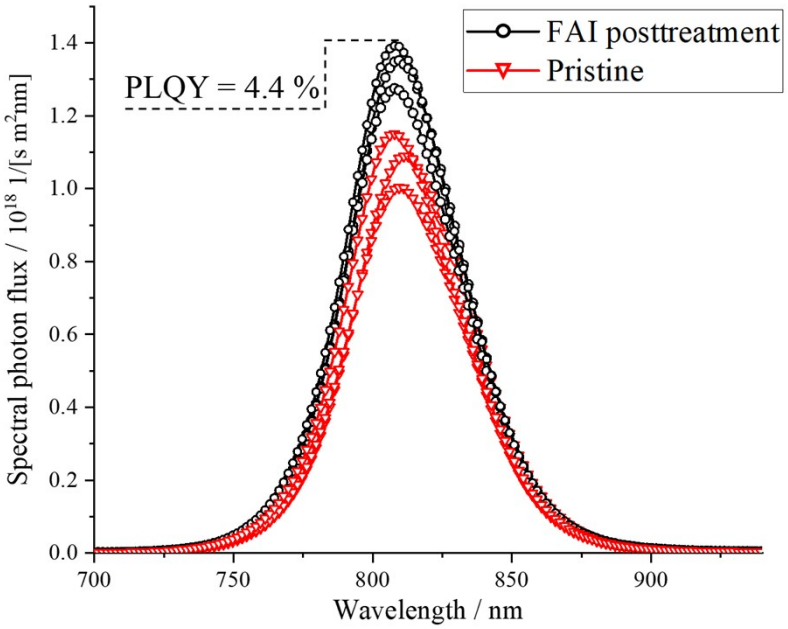

Figure SI 13. PLQY measurement of the posttreated and non-treated $FAPbI_3$ films.

Sample	A	PLQY	PL peak (nm)	E_g(eV)	$V_{oc,\,sq}$ (V)	ΔV (V)	$\Delta E_F/q$ (V)
1_FAI_post	73%	4.35E-02	809	1.533	1.251	-0.081	1.170
2_ FAI_post	73%	4.22E-02	809	1.533	1.250	-0.081	1.169
3_ FAI_post	74%	4.01E-02	808	1.535	1.251	-0.083	1.168
4_no_ FAI_post	77%	3.59E-02	807	1.536	1.251	-0.085	1.166
5_no_ FAI_post	68%	3.45E-02	812	1.526	1.245	-0.086	1.159
6_no_ FAI_post	72%	3.19E-02	809	1.532	1.249	-0.089	1.160

Legend:

- FAI_post : FAI posttreatment approach
- A: Absorptance
- PLQY: Photoluminescence quantum yield
- PL peak: position of PL peak, can be used to determine the band gap
- E_g: Band gap
- $V_{oc,\,sq}$: Shockley-Queisser limit of V_{oc}

- ΔV: Voltage loss due to non-radiative recombination: $\Delta V = k_B T/q\ ln(PLQY)$

Calculation of the quasi-Fermi level splitting To calculate we used the PLQY measurements and the following equation:[98]

$\Delta E_F = q\ V_{oc,rad} + k_B T\ ln(PLQY)$

where is the elementary charge, is the radiative limit of , the Boltzmann constant and T = 25 °C the sample temperature. is calculated by the equation:[98]

$$V_{oc,\,rad} = \frac{k_B T}{q} \ln\left(\frac{J_{sc}}{J_{rad,\,0}} + 1\right)$$

$$J_{rad,0} = q\int_0^\infty a(E)\ \Phi_{BB}(E)dE$$

Here, J_{sc} is the measured photocurrent, the dark emission current and

$$\Phi_{BB}(E) = \frac{1}{4\,\pi^2\,\hbar^3\,c^2}\frac{E^2}{\exp\left(E/(k_B\,T)\right) - 1}$$

the blackbody radiation. The absorptance *a*(E) is derived from the PL spectra by applying the detailed balance principle: [99–101]

Table SI 5. PLQY parameters of the $FAPbI_3$ films.

Sample	$K^{SRH}{}_{eff}$ / 10^5 1/s	(ns)
1_ FAI_post	2.58	1440
2_ FAI_post	3.69	1230
3_ FAI_post	3.77	1150
4_no_ FAI_post	4.63	1080
5_no_ FAI_post	5.29	946
6_no_ FAI_post	6.50	869

Table SI 6. TRPL parameters of the $FAPbI_3$ films with and without FAI surface treatment. A monoexponential fitting was used to determine the given parameters.

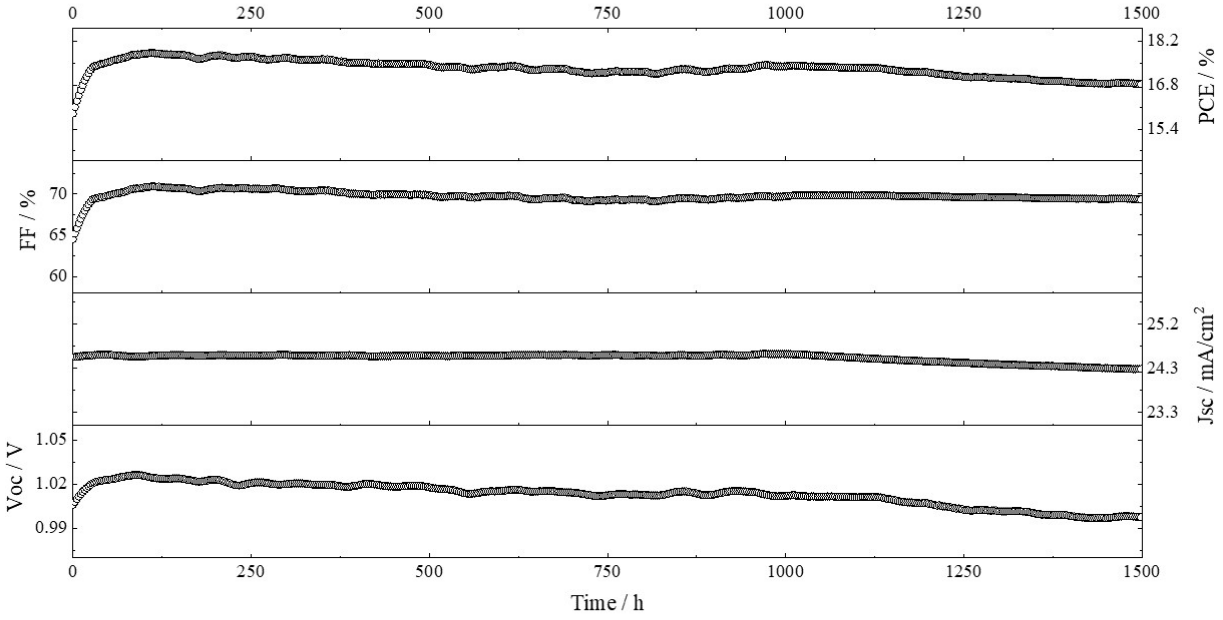

Figure SI 14. Evolution of the PV parameters of the champion cell collected during 1500 h.

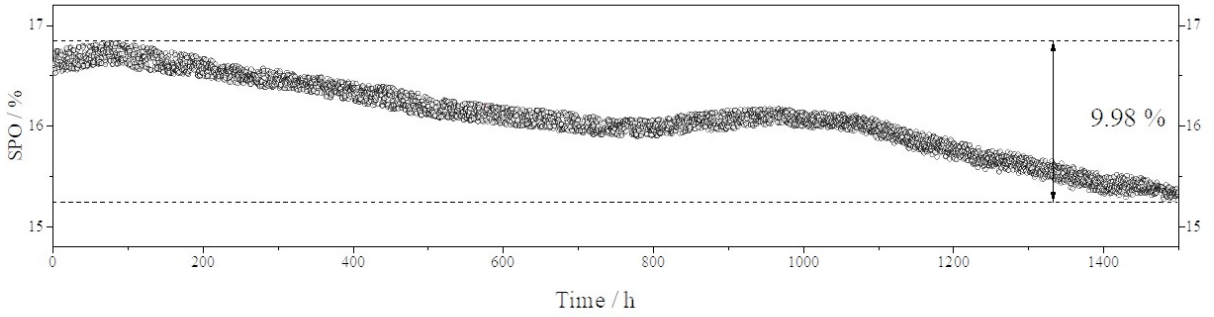

Figure SI 15. SPO for the champion PSC.

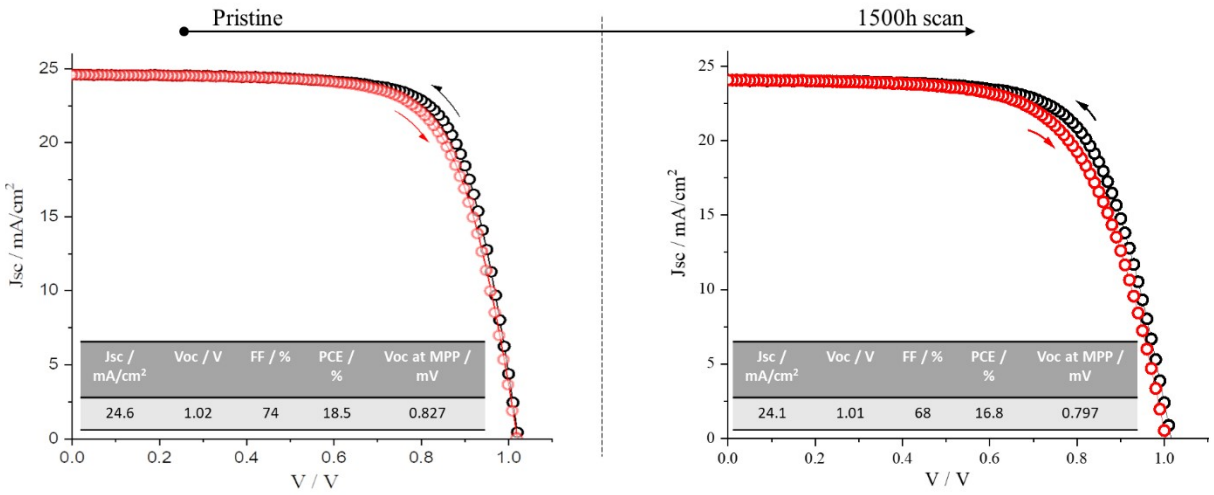

Figure SI 16. [MG1] [SAS2] *JV* curves of the $FAPbI_3$-based champion device *before* and *after* the 1500 h operational stability test. Devices were subjected to continuous MPP tracking while kept under nitrogen at a temperature of 35 °C and exposed of full sunlight intensity. After the 1500 h long test the sample was stored in the dark in a dry box for 1 day, and prior to the measurement of the final JV curve.

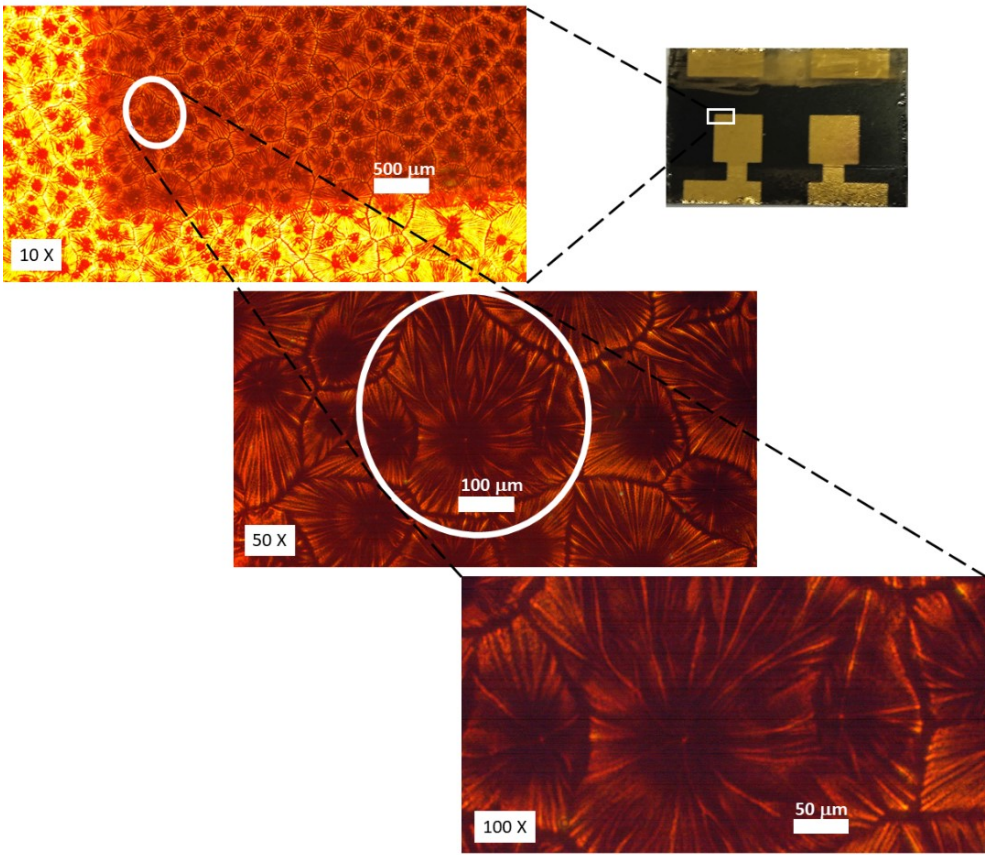

Figure SI 17. Optical image taken in transmission mode at different scales of a perovskite film surface in the active area of a manufactured solar cell.

SI References

97. Ross, R. T. Some Thermodynamics of Photochemical Systems. *The Journal of Chemical Physics* vol. 46 4590–4593 (1967).
98. Rau, U. Reciprocity relation between photovoltaic quantum efficiency and electroluminescent emission of solar cells. *Physical Review B* vol. 76 (2007).
99. Tress, W. Perovskite Solar Cells on the Way to Their Radiative Efficiency Limit - Insights Into a Success Story of High Open-Circuit Voltage and Low Recombination. *Advanced Energy Materials* vol. 7 1602358 (2017).
100. Wurfel, P. The chemical potential of radiation. *Journal of Physics C: Solid State Physics* vol. 15 3967–3985 (1982).
101. Kirchartz, T., Márquez, J. A., Stolterfoht, M. & Unold, T. Photoluminescence-Based Characterization of Halide Perovskites for Photovoltaics. *Advanced Energy Materials* vol. 10 1904134 (2020).